




Communication

A Broad Spectral Photodetector Using Organic Bisindolo Quinoxaline on ZnO Nanorods

Ming-Hsien Li ¹, Yao-Hong Huang ¹, Chi-Chih Chuang ¹, Sang-Hao Lin ¹, Yi-Hsuan Huang ¹, Chia-Feng Lin ²,
Yung-Sen Lin ³, Ming-Yu Kuo ⁴ and Hsiang Chen ^{1,*}

¹ Department of Applied Materials and Optoelectronic Engineering, National Chi Nan University, Nantou 545301, Taiwan

² Department of Materials Science and Engineering, National Chung Hsing University, Taichung 402202, Taiwan

³ Department of Chemical Engineering, Feng Chia University, No. 100, Wenhwa Road, Taichung 407102, Taiwan

⁴ Department of Applied Chemistry, National Chi Nan University, Puli 545301, Taiwan

* Correspondence: hchen@ncnu.edu.tw

Abstract: Inorganic/organic hybrids of ZnO nanorods (NRs)/bisindolo quinoxaline (BIQ) were fabricated for broadband photosensing applications. Multiple material characterizations revealed the BIQ was self-assembled in a regular form of rod-like domain and an irregular form of amorphous aggregation that were distributed on the ZnO NRs. Optical measurements showed that BIQ can absorb visible light with a wavelength up to 630 nm and effectively generate photoelectrons. Moreover, clustering of BIQ can be observed via the 3D optical microscopy. ZnO/BIQ hybrids were promising for future UV and visible light environmental monitoring applications.

Keywords: broadband light sensing; organic BIQ; ZnO nanorods; aggregation; photoluminescence



Citation: Li, M.-H.; Huang, Y.-H.; Chuang, C.-C.; Lin, S.-H.; Huang, Y.-H.; Lin, C.-F.; Lin, Y.-S.; Kuo, M.-Y.; Chen, H. A Broad Spectral Photodetector Using Organic Bisindolo Quinoxaline on ZnO Nanorods. *Chemosensors* **2023**, *11*, 199. <https://doi.org/10.3390/chemosensors11030199>

Academic Editor: Filippo Giubileo

Received: 3 February 2023

Revised: 10 March 2023

Accepted: 16 March 2023

Published: 20 March 2023



Copyright: © 2023 by the authors. Licensee MDPI, Basel, Switzerland. This article is an open access article distributed under the terms and conditions of the Creative Commons Attribution (CC BY) license (<https://creativecommons.org/licenses/by/4.0/>).

1. Introduction

ZnO-based photodetectors (PDs) with a spectral detection ranging from ultraviolet (UV) to visible light have been intensively investigated [1]. Owing to the wide bandgap of 3.4 eV [2], photon energy around the bandgap can be converted to electrical signals for pure ZnO materials. Currently, ZnO-based UV photodetectors [3,4] are promising for environmental hazardous UV light monitoring [5]. However, the wide-bandgap optical properties prevent the ZnO-based optoelectronic devices [6] from being utilized for versatile applications such as imaging and communication, which demand long-wavelength visible light detection. Therefore, researchers have devoted effort to extend the spectral response of ZnO-based PDs [7] by incorporating various materials, such as nanoparticles (NPs) [8], perovskite [9], quantum dots (QDs) [10], and organic compounds [11,12]. Among these additive materials, organic compounds have the advantage of easy fabrication, low cost, and stable response to light illumination. Within three years, different organic compounds, such as PCDTBT [13], PDI, and BIQ-TIPs [14,15], have been proved to enhance the spectral response of ZnO-based PDs. Especially, BIQ-TIPs have self-aggregation effects on the ZnO nanorods (NRs) [16] and enhance the spectral sensing capability for the PDs based on ZnO/ZnS nanostructures [17,18]. Inside the BIQ-TIPs' molecule, there are 4 TIPs moieties connected to the BIQ. The annex of TIPs has the advantage of solubility improvement but the disadvantage of thermal instability. When the BIQ-TIPs are operated at a high temperature of around 100 °C, the bonds between TIPs and BIQ may be broken [19,20], and the degraded BIQ-TIPs further deteriorate the BIQ-TIPs/ZnO hybrid material's chemical and optical properties. In contrast to the thermal instability of

BIQ-TIPs, BIQ has better sensing performance because there is no risk of TIP bonds breaking. Without TIPs, the organic compound of BIQ can have better stability and improve the performance of ZnO-based PDs.

Until now, addition of BIQ (without TIPs) on the ZnO nanorods to fabricate BIQ/ZnO PDs have not been clearly reported yet. In this study, BIQ/ZnO NRs materials were prepared by spreading BIQ on top of ZnO NRs. Multiple material analyses and photoresponse measurements were performed on the BIQ/ZnO NRs devices. Material characterizations revealed that regular and irregular shape of BIQ domain can be formed on top of ZnO NRs, presenting a totally different surface morphology as compared with the BIQ-TIPs/ZnO NRs counterpart. Furthermore, devices using pure BIQ/ZnO NRs exhibited a broader spectral sensing range (up to 630 nm; red light) than that using BIQ-TIPs/ZnO NRs (up to 500 nm; green light). BIQ/ZnO hybrid PDs had potential for future full visible light sensing applications.

2. Materials and Methods

The ZnO/BIQ hybrid materials were prepared on sensing chips, which were based on a SiO₂/SiO substrate (area of 2 × 2 cm²) with an interdigitated electrode (area of 1 × 1 cm²). The substrate was spin-coated with a ZnO seed layer and followed by the hydrothermal growth of ZnO NRs on the seed layer. After the deposition of ZnO NRs, 6,6'-dioctyl-bisindolo[2,3-b]quinoxaline (BIQ) was condensed in chloroform and different quantities of drops (0, 1, 3, and 5 drops) of BIQ solution were drop-casted on top of ZnO NRs. To characterize the presence and clearly view the regular BIQ domain, the sample of ZnO NRs with one drop of BIQ was selected for the morphology analysis. Different amounts of BIQ drops on top of ZnO-NRs-based photodetector are compared to optimize the photosensing capability of BIQ/ZnO-NRs-based photodetector. The molecular structure of BIQ is shown in Figure 1a and is compared with that of BIQ-TIPs in Figure 1b. The flow of the fabrication process is shown in Figure 1c.

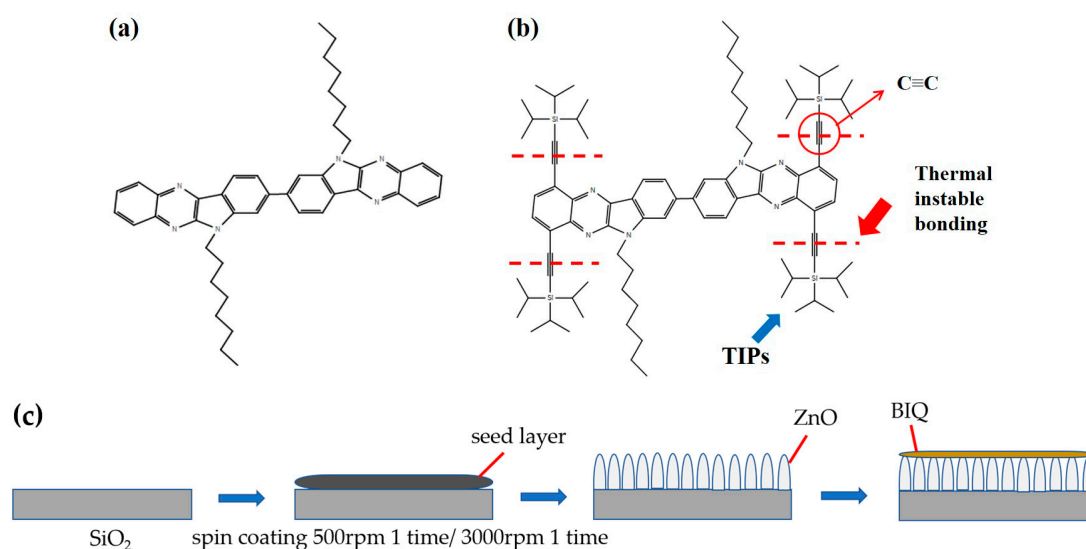


Figure 1. Chemical structure of (a) BIQ and (b) BIQ-TIPs. The TIPs moiety is marked by the red dashed lines. (c) The flow of the fabrication process.

To perform the photosensing measurements, the devices were illuminated with a light source that was switched on and off in a 30 s period. UV LED (peak wavelength at 365 nm), green LED (peak wavelength at 500 nm), red LED (peak wavelength at 630 nm), and white LED were used as the light sources. The sensitivity (S) of a sensing chip was calculated by the following equation:

$$S(\%) = [(I_{\text{light}} - I_{\text{dark}}) / (I_{\text{dark}})] \times 100\% \quad (1)$$

where I_{light} and I_{dark} are the photocurrent and dark current of the devices, respectively.

To characterize the material properties of BIQ/ZnO hybrids, various material analysis techniques including field emission scanning electron microscopy (FESEM), energy-dispersive X-ray spectroscopy (EDX), transmission electron microscopy (TEM), photoluminescence (PL) spectra and images, X-ray diffraction (XRD), confocal laser scanning microscopy (CLSM), and color 3D laser scanning microscopy were used. JEOL JSM-7500F and JEOL JEM 2100 PLUS instruments were utilized to take the FESEM and TEM images, respectively. The SEM and TEM operating voltages were 200 kV and 15 kV, respectively. XRD data were gathered using a discover micro diffractometer (Bruker D8). CLSM images were obtained from inverted confocal microscopy (Carl Zeiss LSM700), while UV/Vis measurements were collected using HITACHI U-3900. Color 3D laser scanning microscope images were obtained through the utilization of KEYENCE VK-9710 K.

3. Results and Discussion

FESEM was first conducted to examine the surface and cross-sectional morphology of BIQ/ZnO hybrids. Figure 2a showed the top-view SEM image of pure BIQ on the SiO₂/Si substrate for comparison. The SEM image revealed plenty of BIQ in a regular rod-like domain clustering on the SiO₂/Si substrate. The top-view and side-view SEM images of BIQ on the ZnO NRs were shown in Figure 2b,c, respectively. Compared with the BIQ/SiO₂, BIQ/ZnO NRs exhibited fewer BIQ domains on the ZnO NRs, presumably owing to the high surface energy of ZnO NRs. The top-view image in Figure 2b showed large rod-like domains of BIQ that were sparsely distributed on top of ZnO NRs. In addition, there were irregular domains of amorphous aggregations in between the ZnO NRs as shown in the top-view and side-view images. Furthermore, a top-view FESEM image with a high magnification rate, shown in Figure 2d, revealed the presence of a regular BIQ domain with a rod-like shape and an irregular BIQ domain of amorphous aggregations, as indicated by two red dash line. The schematic illustration of BIQ depositions on ZnO NRs was shown in Figure 2e, which revealed that most BIQ domains present on top of ZnO NRs exhibited a rod-like shape, while irregular, amorphous BIQ domains were present in between the ZnO NRs.

Compared with our previous work, which was based on the BIQ-TIPs/ZnO NRs, larger and regular BIQ domains can be seen for pure BIQ coated on ZnO NRs because TIPs moieties in the BIQ-TIPs molecule can increase the solubility of BIQ-TIPs in the chloroform. When the BIQ-TIPs precursor was coated on ZnO NRs, the high solubility of BIQ-TIPs decreased the crystallization rate of BIQ-TIPs during chloroform evaporation, resulting in a small BIQ-TIPs domain on the ZnO NRs. XRD profiles of pure BIQ on the SiO₂ substrate and on the ZnO NRs were shown in Figure 3. The characteristic peak at 21° can be assigned to the BIQ (indicated by the red arrow).

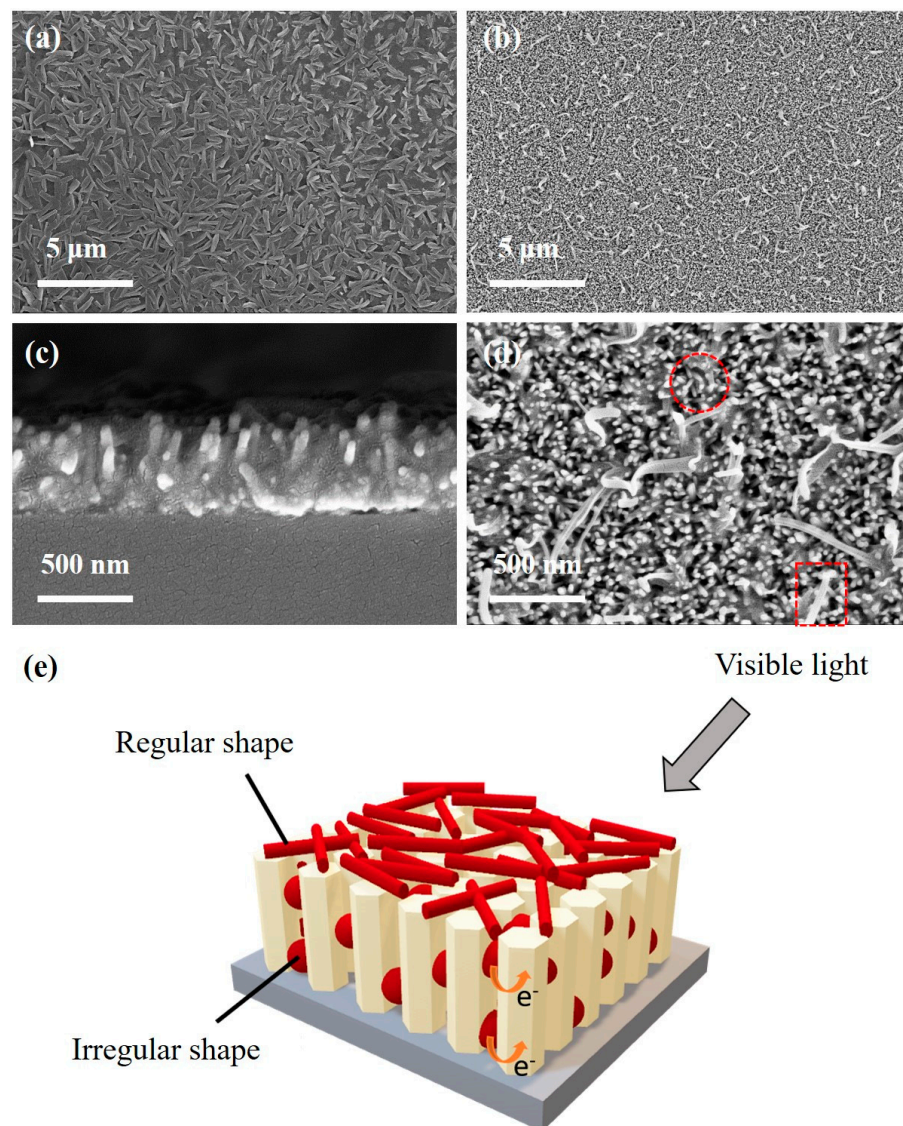


Figure 2. (a) Top-view SEM image of BIQ on a SiO_2/Si substrate. (b) Top-view and (c) cross-sectional SEM image of BIQ/ZnO NRs. (d) Magnified top-view SEM image of (c). (e) Schematic illustration of BIQ/ZnO NRs.

To further examine the fine nanostructures of BIQ/ZnO hybrids, TEM was used as shown in Figure 4a; the TEM image overlapping with EDX mapping was shown in Figure 4b. The TEM image in Figure 4a revealed a rod-shaped ZnO NR overlapping with high-contrast areas. These high-contrast areas may be related to the organic materials owing to their low density. The TEM image with element mapping of Si, Zn, O, and C was presented in Figure 4b. The EDX mapping of Zn and O elements revealed a low contrast on the left side, and the EDX mapping of C has an evenly distributed signal. The results suggested the coverage of organic materials on the ZnO NRs at these low-contrast areas.

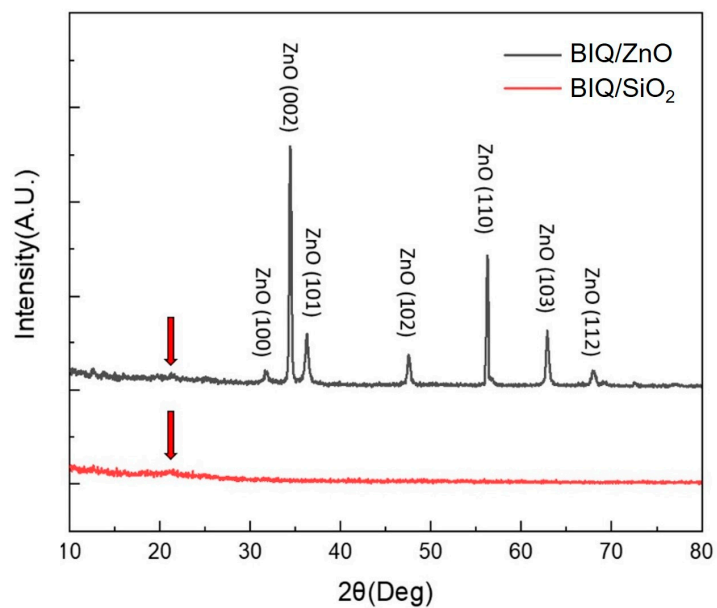


Figure 3. The XRD profile of BIQ deposited on the SiO₂ substrate and the ZnO NRs. The red arrows indicate the characteristic XRD peak of BIQ.

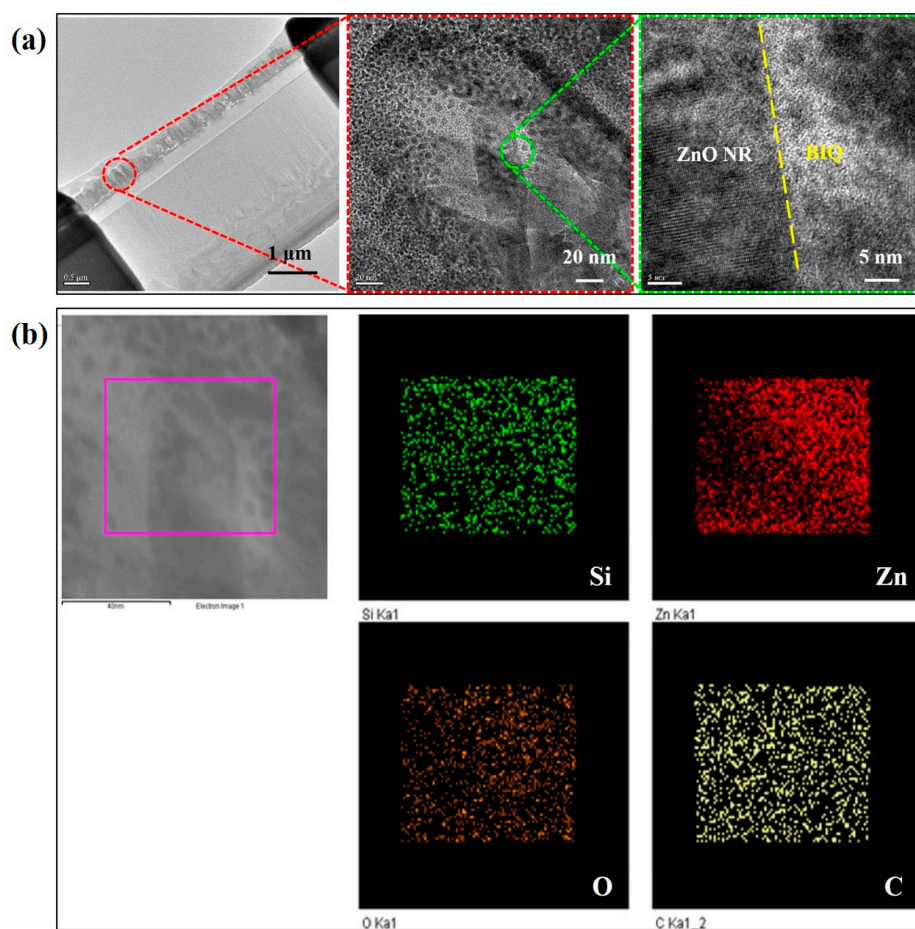


Figure 4. (a) The TEM images of BIQ/ZnO NRs. (b) The TEM image with Si, Zn, O, and C element mapping.

Furthermore, the CLSM was used to macroscopically locate the distribution of BIQ on top of ZnO NRs by receiving the characteristic PL wavelength of BIQ. CLSM mapping images for BIQ on the SiO₂ substrate and for BIQ on the ZnO NRs were shown in Figure 5a,b, respectively, by receiving the PL emission wavelength ranging from 510 to 810 nm was used, while the inset in Figure 5a,b revealed the PL image of BIQ on the SiO₂ and of BIQ on the ZnO NRs, respectively, by receiving the PL emission wavelength ranging from 350 to 510 nm. The PL images of BIQ/SiO₂ revealed that the bright image mainly resulted from the densely distributed BIQ, since the receiving wavelength overlapped well with the characteristic PL emission profile of BIQ. By contrast, the PL image of BIQ/ZnO NRs in Figure 5b unveiled smaller bright regions compared to that of BIQ/SiO₂. The CLSM results also confirmed a smaller surface coverage of BIQ on the ZnO NRs, which was consistent with the results obtained from the SEM image in Figure 2b. These bright regions were ascribed to the presence of sparsely distributed BIQ on the ZnO NRs. The inset in Figure 5b presented the PL image of BIQ/ZnO NRs which was obtained by receiving a PL wavelength ranging from 350 to 510 nm which covered the near-band-edge PL emission of ZnO NRs, while the defect luminescence should be around 550 nm [21]. The corresponding PL image showed a low-brightness region that was ascribed to the ZnO NRs. Moreover, the low PL intensity resulting from the ZnO NRs suggested effective charge transport from ZnO NRs to BIQ and the charge in BIQ underwent radiative recombination to produce the PL emissions beyond 350–510 nm. Figure 5c–e showed the PL image of BIQ/ZnO NRs probed at different positions; the corresponding PL emission profile was revealed in Figure 5f. The results indicated that the main emission wavelength of BIQ/ZnO NRs was within 450–800 nm, with a PL emission peak at around 600 nm. The PL emission peak of ZnO NRs defect state was at around 550 nm. The shifted PL emission peak of BIQ/ZnO NRs also suggested the charge transfer from ZnO NRs to BIQ.

Moreover, to investigate the surface clustering effect, color 3D laser scanning microscopy was used. The color 3D images for BIQ/ZnO and BIQ/SiO₂ were shown in Figure 6a,b, respectively. Compared with deposition of BIQ on the SiO₂ substrate as shown in Figure 6b, deposition of BIQ on the ZnO NRs exhibited a nonuniform surface morphology, which indicated the aggregation of BIQ on pure ZnO NRs. However, the aggregation effect of BIQ on the ZnO NRs was not as strong as that of BIQ-TIP on the ZnO NRs, which may result from high solubility of BIQ-TIP induced by the four TIPs moieties.

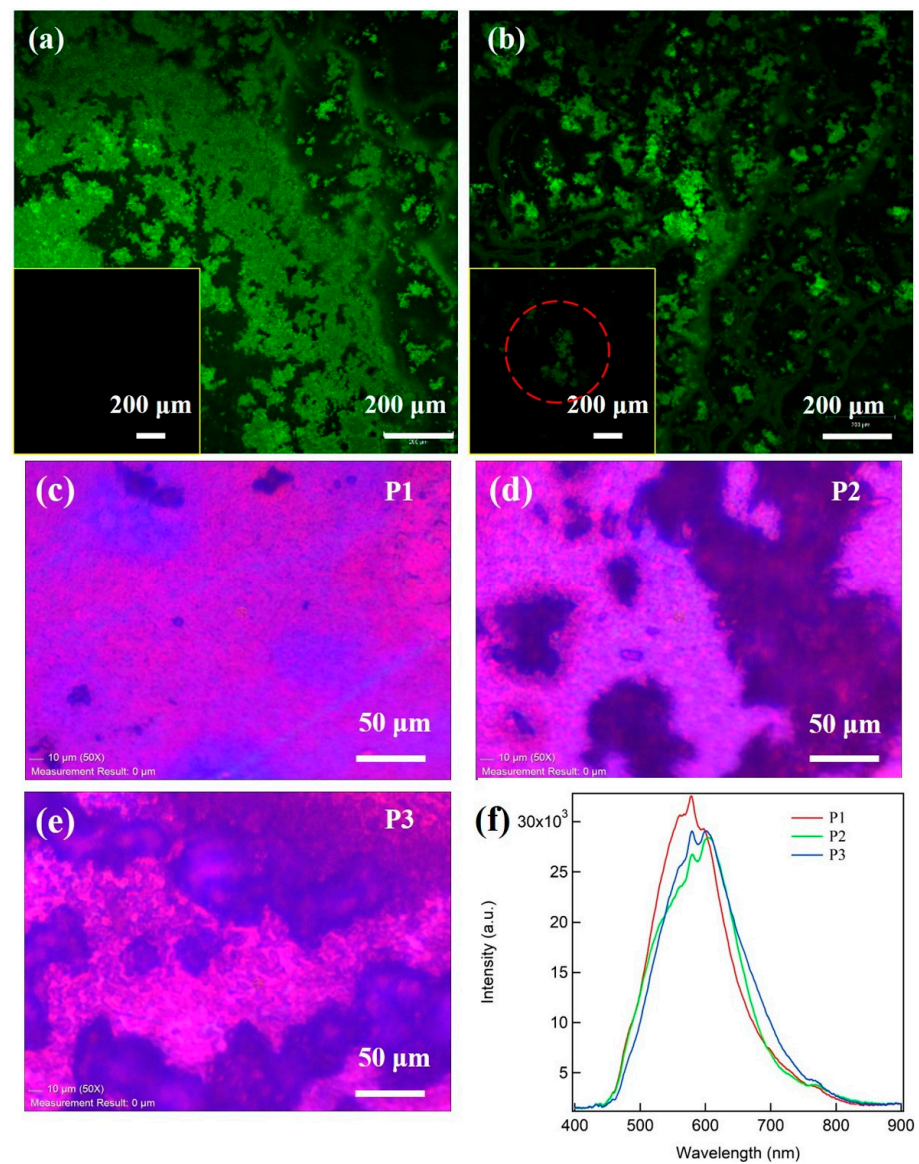


Figure 5. The CLSM images of (a) BIQ/SiO₂ and (b) BIQ/ZnO NRs samples. The PL receiving wavelength range is from 510 to 810 nm. The subfigure in (a,b) corresponds to the CLSM image when receiving the PL wavelength with a range of 350–510 nm. The PL image of BIQ/ZnO NRs sample when (c) P1, (d) P2, and (e) P3 are in different positions. (f) The corresponding PL emission spectrum at P1–P3.

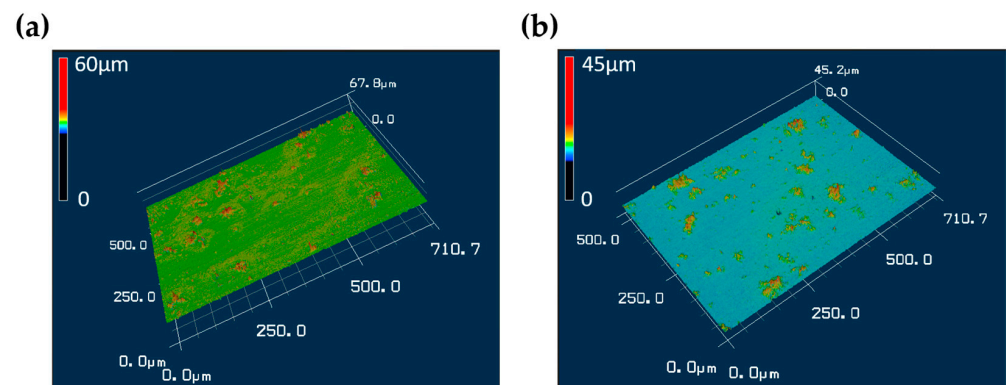


Figure 6. The Color 3D confocal images of (a) BIQ/ZnO NRs and (b) BIQ/SiO₂.

Finally, the photosensing performance of BIQ/ZnO NRs devices under the UV-, white-, green-, and red-LED illumination was shown in Figure 7a. The light intensity of various LED sources was shown in Table 1. To optimize the photosensing performance of BIQ/ZnO NRs device, deposition of BIQ precursor with different drops (1, 3, and 5 drops) on the ZnO NRs was performed. Figure 7a presented the photosensing behavior of pure ZnO NRs devices and BIQ/ZnO NRs devices with different amounts of drops of BIQ precursor in response to the UV-LED illumination. Devices with 3 drops of BIQ had the strongest photoresponse among all the samples, while devices with pure ZnO NRs had the shortest response and recovery time. When the BIQ covered the ZnO NRs, most UV light was absorbed by the outer BIQ and converted into photoelectrons that required time to undergo charge transfer from the organic BIQ to the ZnO NRs. For the pure ZnO-NRs-based devices illuminated with green LED, white LED, and red LED, a low photoresponse or even noise was detected as compared with the BIQ/ZnO NRs counterpart. Among the BIQ/ZnO NRs devices with various BIQ drops, the devices with 3 drops had a better photoresponse than that with 5 drops. An excessive amount of BIQ drops may spread more BIQ on top of ZnO NRs and produce thick BIQ domains. These thick BIQ domains strongly absorbed the illuminated light and reduced the light absorbed by the ZnO NRs. As a result, low photogenerated carriers in the ZnO NRs could decrease the photoconductivity and further deteriorate the device photoresponse. It was noted that devices with BIQ-TIPs exhibited photoresponse only up to green light (around 500 nm), while they had a negligible response in red light. By contrast, devices with BIQ were capable of red-light detection as seen in Figure 7d. The extension of the spectral response for the BIQ/ZnO NRs based devices may result from the lower bandgap of BIQ compared with that of BIQ-TIPs. Without the four TIPs bonding to the BIQ molecules, the interlayer stacking of BIQ is closer than that of BIQ-TIPs to reducing the bandgap of BIQ. The sensitivity of BIQ/ZnO NRs devices was better than that of BIQ-TIPs/ZnO NRs devices under UV and green LED illumination as shown in Table 2.

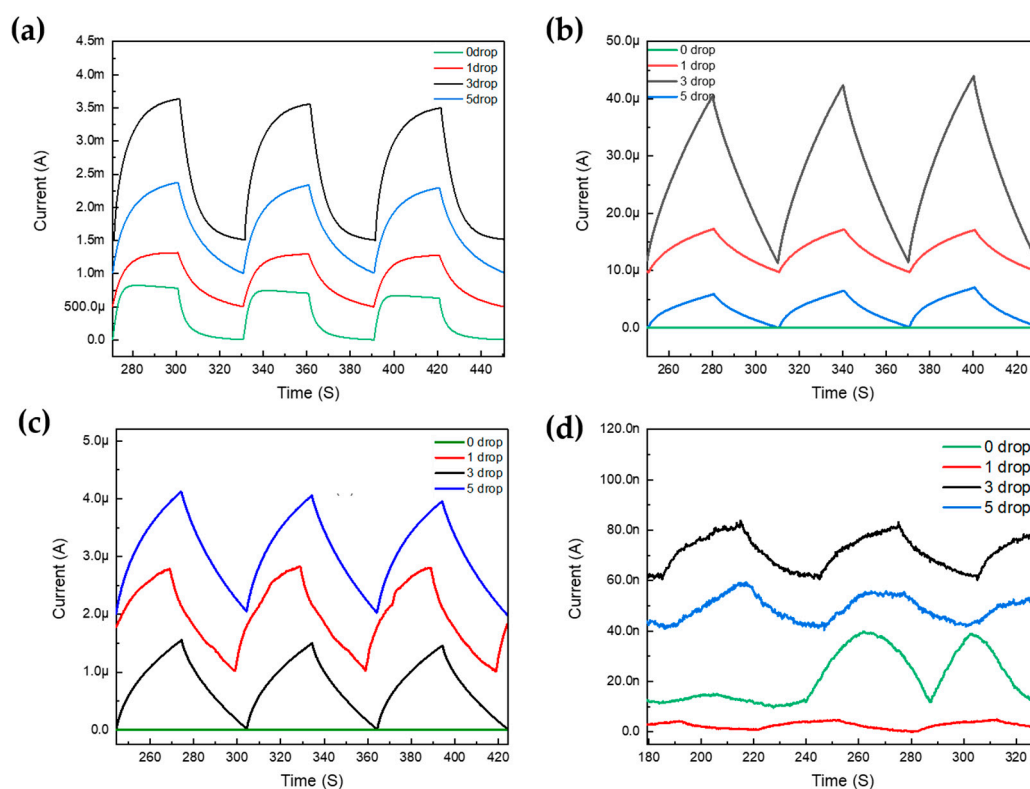


Figure 7. The photoresponse of ZnO NRs photodetector with various amounts of drops (0, 1, 3, and 5 drops) of BIQ solution under (a) UV, (b) white, (c) green, and (d) red LED illumination.

Table 1. The light intensity of various LED sources.

UV LED	White LED	Green LED	Red LED
22.2 W/m ²	46.67 W/m ²	41.67 W/m ²	33.3 W/m ²

Table 2. Comparison of photosensitivity of BIQ/ZnO NRs and BIQ-TIPs/ZnO NRs devices under UV and green LED illumination.

	UV LED	Green LED
BIQ/ZnO NRs PDs	800.3%	12.3%
BIQ-TIPs/ZnO NRs PDs	169.4%	5.3%

4. Conclusions

In this study, ZnO NRs with organic BIQ spread on top of them were fabricated on sensing chips to function as broadband photodetectors. Incorporation of BIQ into the ZnO-NRs-based device can enhance the photoresponse and extend the spectral response compared with the pure ZnO NRs counterpart. Multiple material characterizations revealed that BIQ formation in regular-shape domains and irregular domains were distributed on the ZnO NRs. PL images indicated that organic BIQ mainly emits long PL wavelength at around 600 nm. Application of inorganic/organic ZnO/BIQ hybrids for photodetector were promising for broadband photosensing that covered UV and visible light.

Author Contributions: Conceptualization, M.-H.L., M.-Y.K. and H.C.; methodology, C.-C.C., Y.-H.H. (Yao-Hong Huang), S.-H.L. and Y.-H.H. (Yi-Hsuan Huang); software, C.-C.C., Y.-H.H. (Yao-Hong Huang), S.-H.L. and Y.-H.H. (Yi-Hsuan Huang); data curation, C.-C.C., Y.-H.H. (Yao-Hong Huang), S.-H.L. and Y.-H.H. (Yi-Hsuan Huang); writing—original draft preparation, M.-H.L., M.-Y.K. and H.C.; writing—review and editing, M.-H.L., M.-Y.K. and H.C.; visualization, H.C.; supervision, C.-F.L. and Y.-S.L.; project administration, H.C.; funding acquisition, M.-H.L., M.-Y.K. and H.C. All authors have read and agreed to the published version of the manuscript.

Funding: This research was funded by the Ministry of Science and Technology (MOST), Taiwan, grant number “110-2221-E-260-006-”, “109-2222-E-260-001-MY3” and “The APC was funded by the National Chi Nan University”.

Institutional Review Board Statement: Not applicable.

Informed Consent Statement: Not applicable.

Data Availability Statement: Not applicable.

Conflicts of Interest: There are no conflict of interest to declare. The funders had no role in the design of the study; in the collection, analyses, or interpretation of data; in the writing of the manuscript, or in the decision to publish the result.

References

- Chen, J.; Ouyang, W.; Yang, W.; He, H., Jr.; Fang, X. Recent progress of heterojunction ultraviolet photodetectors: Materials, integrations, and applications. *Adv. Funct. Mater.* **2020**, *30*, 1909909.
- Singh, J.; Kaur, S.; Kaur, G.; Basu, S.; Rawat, M. Biogenic ZnO nanoparticles: A study of blueshift of optical band gap and photocatalytic degradation of reactive yellow 186 dye under direct sunlight. *Green Process. Synth.* **2019**, *8*, 272–280.
- Liu, K.; Sakurai, M.; Aono, M. ZnO-based ultraviolet photodetectors. *Sensors* **2010**, *10*, 8604–8634. [[CrossRef](#)] [[PubMed](#)]
- Ouyang, W.; Chen, J.; Shi, Z.; Fang, X. Self-powered UV photodetectors based on ZnO nanomaterials. *Appl. Phys. Rev.* **2021**, *8*, 031315.
- Kao, C.H.-L.; Nguyen, B.; Roseway, A.; Dickey, M. Earthtones: Chemical sensing powders to detect and display environmental hazards through color variation. In Proceedings of the 2017 CHI Conference Extended Abstracts on Human Factors in Computing Systems (CHI EA’17). Association for Computing Machinery, New York, NY, USA, 6–11 May 2017; pp. 872–883.
- Fortunato, E.M.C.; Barquinha, P.M.C.; Pimentel, A.C.M.B.G.; Gonçalves, A.M.F.; Marques, A.J.S.; Martins, R.F.P.; Pereira, L.M. Wide-bandgap high-mobility ZnO thin-film transistors produced at room temperature. *Appl. Phys. Lett.* **2004**, *85*, 2541–2543. [[CrossRef](#)]

7. Panwar, V.; Nandi, S.; Majumder, M.; Misra, A. Self-powered ZnO based pyro-phototronic photodetectors: Impact of heterointerfaces and parametric studies. *J. Mater. Chem. C* **2022**, *10*, 12487–12510.
8. Mitchell, M.J.; Billingsley, M.M.; Haley, R.M.; Wechsler, M.E.; Peppas, N.A.; Langer, R. Engineering precision nanoparticles for drug delivery. *Nat. Rev. Drug Discov.* **2021**, *20*, 101–124. [[CrossRef](#)] [[PubMed](#)]
9. Qin, W.; Yuan, Z.; Gao, H.; Zhang, R.; Meng, F. Perovskite-structured LaCoO₃ modified ZnO gas sensor and investigation on its gas sensing mechanism by first principle. *Sens. Actuators B Chem.* **2021**, *341*, 130015. [[CrossRef](#)]
10. de Arquer, F.P.G.; Talapin, D.V.; Klimov, V.I.; Arakawa, Y.; Bayer, M.; Sargent, E.H.; Baggiolini, A.; Callahan, S.J.; Luo, L.; Zuko, A.; et al. Semiconductor quantum dots: Technological progress and future challenges. *Science* **2021**, *373*, eaaz8541. [[CrossRef](#)] [[PubMed](#)]
11. Yuan, Z.; Han, E.; Meng, F.; Zuo, K. Detection and identification of volatile organic compounds based on temperature-modulated ZnO sensors. *IEEE Trans. Instrum. Meas.* **2019**, *69*, 4533–4544. [[CrossRef](#)]
12. Manjari, G.; Saran, S.; Radhakrishnan, S.; Rameshkumar, P.; Pandikumar, A.; Devipriya, S.P. Facile green synthesis of Ag–Cu decorated ZnO nanocomposite for effective removal of toxic organic compounds and an efficient detection of nitrite ions. *J. Environ. Manag.* **2020**, *262*, 110282. [[CrossRef](#)] [[PubMed](#)]
13. Zhang, Z.-S.; Liu, J.-X.; Cheng, X.-F.; He, J.-H.; Li, H.; Xu, Q.-F.; Li, N.-J.; Chen, D.-Y.; Lu, J.-M. Ultrasensitive humidity sensing using one-dimensional π -d conjugated coordination polymers for breath monitoring. *Sens. Actuators B Chem.* **2020**, *330*, 129353. [[CrossRef](#)]
14. Li, M.-H.; Liang, K.-T.; Wu, Z.-H.; Lin, S.-H.; Chiu, Y.-S.; Lee, C.-H.; Kuo, M.-Y.; Lin, C.-F.; Chen, H.; Wu, D.-S.; et al. Synergetic Effects of ZnS Core Shell and Bisindolo Quinoxaline-Tips (BIQ-TIPs) Spreading on ZnO Nanorod-Based Light/Gas Dual Sensors. *IEEE Sens. J.* **2022**, *22*, 23821–23828. [[CrossRef](#)]
15. Ytsai, Y.-S.; Chen, C.-J.; Huang, Y.-T.; Liang, K.-T.; Jhang, J.-J.; Huang, S.-H.; Li, M.-H.; Wu, Y.S.; Kuo, M.-Y.; Chen, H.; et al. Incorporation of hydrophobic-like bisindolo quinoxaline-tips (BIQ-TIPs) aggregation on ZnO nanorods for spectral broadening photodetection. *Results Phys.* **2022**, *34*, 105318.
16. Liu, X.; Chen, C. Mxene enhanced the photocatalytic activity of ZnO nanorods under visible light. *Mater. Lett.* **2019**, *261*, 127127. [[CrossRef](#)]
17. Yang, X.; Liu, H.; Li, T.; Huang, B.; Hu, W.; Jiang, Z.; Chen, J.; Niu, Q. Preparation of flower-like ZnO@ ZnS core-shell structure enhances photocatalytic hydrogen production. *Int. J. Hydrogen Energy* **2020**, *45*, 26967–26978. [[CrossRef](#)]
18. Zhao, X.; Feng, J.; Liu, J.; Lu, J.; Shi, W.; Yang, G.; Wang, G.; Feng, P.; Cheng, P. Metal–Organic Framework-Derived ZnO/ZnS Heteronanostructures for Efficient Visible-Light-Driven Photocatalytic Hydrogen Production. *Adv. Sci.* **2018**, *5*, 1700590. [[CrossRef](#)] [[PubMed](#)]
19. Montarnal, D.; Capelot, M.; Tournilhac, F.; Leibler, L. Silica-like malleable materials from permanent organic networks. *Science* **2011**, *334*, 965–968. [[CrossRef](#)] [[PubMed](#)]
20. Ohe, T.; Kuribayashi, M.; Yasuda, R.; Tsuboi, A.; Nomoto, K.; Satori, K.; Itabashi, M.; Kasahara, J. Solution-processed organic thin-film transistors with vertical nanophase separation. *Appl. Phys. Lett.* **2008**, *93*, 286. [[CrossRef](#)]
21. Cheng, C.-C.; Weng, W.C.; Lin, H.; Chiu, J.L.; Jhao, H.-Y.; Liao, Y.T.A.; Yu, C.T.R.; Chen, H. Fabrication and characterization of distinctive ZnO/ZnS core–shell structures on silicon substrates via a hydrothermal method. *RSC Adv.* **2018**, *8*, 26341–26348. [[CrossRef](#)] [[PubMed](#)]

Disclaimer/Publisher’s Note: The statements, opinions and data contained in all publications are solely those of the individual author(s) and contributor(s) and not of MDPI and/or the editor(s). MDPI and/or the editor(s) disclaim responsibility for any injury to people or property resulting from any ideas, methods, instructions or products referred to in the content.